J Mater Sci (2006) 41:6925–6937
DOI 10.1007/s10853-006-0217-2

Porosity and water permeability of rice husk ash-blended cement composites reinforced with bamboo pulp

Conrado de Souza Rodrigues · Khosrow Ghavami · Piet Stroeven

Received: 21 December 2004 / Accepted: 7 June 2005 / Published online: 16 September 2006

Abstract Cellulose fibres have already been applied commercially as an alternative to asbestos in fibre-cements composites. In spite of their industrial scale production for more than 20 years, these composites still require much research efforts, which focus mainly on durability aspects. The influence of the most relevant deterioration mechanisms can be minimized if mineral admixtures with high pozzolanic activity replace ordinary Portland cement (OPC). The improvements then achieved are due to the decrease in $Ca(OH)_2$ content and the more compact matrix and interfaces in the composite. In this respect, rice husk ash (RHA) is one of the most promising materials to be applied as a partial cement replacement in the cellulose-reinforced cement-based composites. This is due to the high active silica content of the ash and the widespread availability of the husks. To assess the influences of different chemical compositions of RHA, and the effects of autoclave curing on the pore characteristics of bamboo-pulp-reinforced cement composites, a comparative study was carried out in which pore characteristics were assessed by mercury intrusion porosimetry (MIP). Complementarily, the effects exerted by changes in the pore structure of the composites on their water permeability are evaluated by analytical and experimental approaches. It was observed that the incorporation of RHA in the composites could cause an extensive pore refinement in the matrix and in the interface layer, thereby decreasing water permeability. The results indicate that partial replacement of cement by RHA can improve the durability characteristics of cellulose–cement composites.

C. de Souza Rodrigues (✉)
Department of Civil Engineering, Federal Centre for Technological Education of Minas Gerais - CEFET/MG, Av. Amazonas, 7675, Belo Horizonte, CEP: 30510-000, Minas Gerais, Brazil
e-mail: crodrigues@des.cefetmg.br

K. Ghavami
Department of Civil Engineering, Pontifical Catholic University of Rio de Janeiro, PUC-Rio, Av. Marquês de São Vicente, 225, CEP: 22453-900, Rio de Janeiro, RJ, Brazil
e-mail: ghavami@civ.puc-rio.br

P. Stroeven
Faculty of Civil Engineering and Geosciences, Delft University of Technology, DUT, Stevinweg 1, 2628 CN, Delft, The Netherlands
e-mail: p.stroeven@citg.tudelft.nl

Introduction

Health problems associated with exposure to asbestos have compelled countries since the early 70's to adopt policies restricting the utilization of asbestos-based products. As a consequence, asbestos-cement, one of the most successful building materials, has been banned, or saw its employment restricted in an increasing number of countries. Due to its high mechanical strength, lightweight, durability and low cost, asbestos-cement components still play a key role in low-cost housing projects, mainly in undeveloped and developing countries. In trials to replace this material we should therefore focus both on material behaviour and affordability.

Among the wide range of available fibres as a potential replacement of asbestos, cellulosic pulps have always been considered a viable alternative, when the physical and chemical properties of the matrix, as well as the production process of the composites are adjusted [1]. As a result, cellulosic pulps have been applied on large scale as reinforcement of cementitious composites for more than two

decades [1–3]. These non-hazardous composites present short-term mechanical and physical behaviour compatible to that observed in asbestos-cement for most of the common applications. However, durability characteristics still need considerable research efforts.

Environmental agents, combined with hydration products, activate a range of mechanisms in the high alkalinity environment of the cementitious matrix that modify the properties of the cellulose–cement composites, impairing their long term performance. These mechanisms are fdescribed in detail in the literature [2, 4–8], being the more direct effects on the composite strength due to:

- Interfacial debonding: mainly due to fibre-matrix abrasion that results from cycles of volumetric expansion-shrinkage of the fibres and matrix under temperature and moisture variations.
- Fibres embrittlement: resulting from migration of hydration products to the fibres' pores and lumen.
- Alkali attack: by some of the hydration products causing dissolution of the cellulosic chain.

Since these deterioration mechanisms are strongly dependent on moisture movement through the porous network of the composites, one of the most applied preventive methods is the partial replacement of cement by finely ground mineral admixture with high pozzolanic activity. The improved durability of the composites is due to the lower matrix alkalinity and higher density of matrix and interface layer [4, 7,8], resulting from the pozzolanic reaction, involving $Ca(OH)_2$ consumption, and the filling effect of the pozzolanic materials, respectively. Generally, the addition of pozzolanic admixtures has chemical and physical effects, although they are interrelated. The pozzolanic reaction can be understood in chemical terms as a dissolution-precipitation mechanism, however yielding reaction products smaller than the original admixture and cement particles [9]. These act as filler, improving density and enhancing physical (van der Waals-type of) binding forces.

Rice husk ash (RHA) as a mineral admixture

Rice is a major crop in many world regions, accounting for an estimated production of rice husk as an agricultural residue totalling about 608 million tonnes in 2004 [10]. This amount would allow the generation of about 121 million tonnes of pozzolanic ash. Part of the husk is applied as fuel during rice processing or for domestic cooking in rural areas. However, most of this agricultural by-product is simply disposed in nature representing an environmental problem. Burning rice husks results in ash with high silica content and, when the burning process is carried out properly, the silica in RHA is amorphous, making it a proper cement replacement material due to its high pozzolanic activity [11–13].

RHA is applied in this study as a partial replacement material for OPC in cellulose–cement composites as a mean to obtain materials with improved durability characteristics, which may be accomplished by composites with denser and less permeable matrix and interfaces. Since the RHA properties are very sensitive to the burning process, ashes with different chemical compositions are considered in this study. The composites were produced with different replacement rates and subjected to conventional and accelerated autoclave curing. To evaluate the effects of these variables on the composite structure, a comparative study was carried out applying MIP. The changes in the pore structure due to RHA incorporation influence the transport mechanisms in the composite. Therefore, this study also focused on water permeability of the composites, achieved analytically as well as experimentally. Although only short-term porosity and permeability characteristics are discussed, the modifications in the material structure may indicate improvements in their long-term behaviour.

Porosity of cement-based materials

The porosity of a porous media, ϕ, can be classified in general terms in micro ($d < 0.002$ μm), meso ($0.002 < d < 0.05$ μm) and macro pores ($d > 0.05$ μm) [14, 15], where d is the pore diameter. In cement-based materials, pores larger than 0.05 μm influence strength and permeability, while those smaller govern creep and shrinkage behaviour [16]. In the mesoporosity range, electrostatic interactions occur between the pore walls and the fluid, blocking transport through these pores. Hence, the way mineral admixtures affect the transport properties of cementitious materials can be interpreted in terms of the increased volume of meso pores with a correspondent decrease in that of macro pores [14].

Porosity is determined through MIP by measuring the volume of mercury intruded in the sample under a given pressure. During the intrusion test, the pressure is increased from the atmospheric level to a couple of hundreds MPa, resulting in intrusion curves reflecting pressure data as a function of the intruded volume of mercury. Under the assumption that the pore structure consists of cylindrical pores, the pressure applied to the mercury, P, is given in terms of the pore diameter by the Washburn relation [17].

$$d = \frac{-4.\gamma.\cos\theta}{P} \quad (1)$$

in which θ is the contact angle between mercury and the sample material, and γ is the surface tension of mercury.

MIP test data should be interpreted with great care, accounting for the weak points of the method. Due to the hypothesis of a cylindrical pores network and the uncertainty of the contact angle adopted in Eq. (1), the pore diameters calculated by the Washburn relation will not represent the real values found in the sample [14, 18]. The ''ink-bottle'' pores are represented in the intrusion curves as several small pores, instead of a larger pore with a narrow entrance. A third source of uncertainty in the diameter values calculated by the Washburn relation is the adoption of a single value as material property for the contact angle, θ, for composite samples with bended-matrixes. Direct observation of the pore network of cement pastes by scanning electron microscopy (SEM) resulted in pore size distributions involving pore diameters 100 times larger than those from MIP tests [19], although this approach also involves approximations, with three-dimensional information being obtained from two-dimensional images.

Despite all limitations, MIP is still employed as a standard way to evaluate the pore structure of cement materials [14] and regarded to be well reproducible [19, 20]. The method has shown a valuable tool in this comparative study to evaluate the effects of RHA incorporation in the structure of the cellulose–cement composites.

Permeability determination based on MIP tests

A laminar flow through a porous media can be expressed by Darcy's law,

$$q = \frac{K.\Delta P}{\eta.L} \tag{2}$$

in which q is the flow rate (m^3/s), ΔP is the pressure gradient (N/m^2), L is the length of the sample in the flow direction (m), η is the fluid viscosity (N s/m^2), and K is the permeability of the medium (m^2) [21]. In spite of its simplicity, the application of Eq. (2) for experimental determination of permeability is not an ordinary task, since the laminar flow condition cannot easily be achieved in experiments on low permeability materials. As a consequence, the results usually reveal large discrepancies due to dependence on the equipment and the experimental methodology adopted [22].

The permeability of a medium is a function of its pore structure. Models based on results from MIP tests have quantitatively correlated both. One of these models was developed by Katz and Thompson [23], here referred to as the K–T model and expressed by

$$K = c.d_c^2.\frac{\sigma}{\sigma_o}, \quad \frac{\sigma}{\sigma_0} = \frac{d^e_{m\acute{a}x}}{d_c}\phi.S(d^e_{m\acute{a}x}) \tag{3}$$

Herein, permeability is given in terms of the characteristic diameter of the pore network, d_c, and is σ/σ_0 the relative conductivity, in which σ is the electrical conductivity of a material saturated by a fluid with electrical conductivity σ_0. Finally, c is a constant of about 1/126 [23]. In the intrusion curves obtained from MIP tests, d_c corresponds to the threshold diameter, representing the opening of the interconnected pore network in the sample.

The relative conductivity is related to the connectivity of the pores in the sample and can also be established from MIP data through the second equation in Eq. (3), whereby d^e_{max} is a characteristic dimension associated with maximum conductance. $S(d^e_{max})$ is the porosity due to pores larger than d^e_{max}, and ϕ is the total porosity. For materials presenting a vast range of pore sizes, it is assumed that $d^e_{max} = 0.34d_c$ [21]. The K–T model was originally applied to sedimentary rocks, resulting in calculated permeability data well correlated to values established experimentally [23].

For cement-based materials, it was shown that the calculated values of σ/σ_0 presents good correlation with experimental values obtained through electrical conductivity measurements [24]. However, different attempts reported in the literature have shown that the K–T model fails to predict the permeability of those materials, with calculated values being in many cases two orders of magnitude higher than the experimentally values [21, 24–26]. Application of the K–T model to cementitious materials is criticized mainly because porosity is consisting of capillary and gel pores, so that a single material parameter, d_c, cannot be used [27]. Therefore permeability model on the basis of capillary and gel pores, by combining these two phases through an effective media theory, was developed by Cui and Cahyadi [26]. In this model, permeability is considered as a function of low and high permeability phases, K_L and K_H, which are related to gel and capillary phases, respectively, Eq. (4).

$$\frac{(1-\phi_{cap})\left(K_L^{1/t}-K^{1/t}\right)}{K_L^{1/t}+AK^{1/t}} + \frac{\phi_{cap}\left(K_H^{1/t}-K^{1/t}\right)}{K_H^{1/t}+AK^{1/t}} = 0 \tag{4}$$

in which ϕ_{cap} is the porosity related to the high permeability phase (pores larger than d_c), $t = 2$ is assumed for three-dimensional pore systems, and $A = (1-\phi_c)/\phi_c$, in which ϕ_c is the critical capillary porosity value defined as 0.18 [28]. It is referred to in this study as the C–C model. The two permeabilities K_L and K_H follow from

$$K_H = c.d_c^2 1.8(1-\phi_c)^2, \quad K_L = K_{CSH}\left(1-\frac{1-\phi_{CSH}}{1-\phi_c'}\right)^2 \tag{5}$$

The permeability of the capillary phase in the first of Eq. (5) is determined neglecting the permeability of the gel phase, and is a function of d_c only [26]. Next, K_L is assessed under the assumption that $K_H = 0$ in Eq. (4), and that the cement paste is composed of C–S–H, CH and unhydrated particles, whereby C–S–H is the only permeable phase. Under such conditions Eq. (4) degenerates to the second of Eq. (5), where K_{CSH} and ϕ'_c are the permeability and the critical volume fraction of the C–S–H phase, respectively, with approximate values of $\phi'_c = 0.17$ and $K_{CSH} = 7.10^{-23}$ m^2 [26, 29].

The volume fraction of C–S–H, ϕ_{CSH}, is the ratio of the volume of C–S–H, V_{CSH}, and the total volume of the three phases, *i.e.*, in addition to C–S–H, CH, and the unhydrated particles. The volumes of hydration products, $V_{CSH} + V_{CH}$, and the volume of unhydrated particles, V_{uH}, are calculated by means of [26, 29]:

$$V_{CSH} + V_{CH} = \frac{0.68\alpha}{w/c + 0.32},$$
$$V_{uH} = \frac{0.32(1-\alpha)}{w/c + 0.32}, \quad (6)$$
$$\alpha = \frac{(1-\phi).w/c - 0.32\phi}{0.36}$$

Materials

RHA

A high-carbon-content RHA (RHA-I) was obtained from Vietnamese rice husks burned for few seconds at temperatures ranging from 500 °C to 750 °C, as the ash pass through a kiln specially developed for this purpose [12]. This high-carbon-content ash represents that resulted from the application of the rice husk as a fuel. A low-carbon-content RHA is produced (RHA-II) upon re-burning part of this ash for 3 h in a conventional kiln at 750 °C. Thereupon, both RHA samples were grounded in a ceramic ball mill for 12 h.

Table 1 presents data on the chemical composition, pozzolanic index ΔmS/cm, specific surface area obtained by N_2 absorption, S_{BET}, and the average particle size of the ashes, δ, determined through the Coulter Counter method [30]. It can be inferred from Table 1 that a reduction of the carbon content in the ash (and increasing the silica content) causes significant modifications in the structure of the RHA grains. RHA-I yields high S_{BET}, which is not only due to the smaller size of its particles, but is mainly the result of the high-carbon-content particles of which the surfaces are reported to be rich in micro porosities and discontinuities [11–13]. Also, it can be concluded that the re-burning process resulted in a harder material, since RHA-II consists of larger particles than RHA-I (Fig. 1), despite both being subjected to the same grinding conditions. The silica structure was also modified by the prolonged incineration period applied to RHA-II, whereby a higher amount of crystalline silica (crystoballite, C) was observed in the X-Ray diffraction tests, as can be observed in Fig.1.

The pozzolanic activity of the ashes was determined by measuring the change in the electrical conductivity of a saturated lime solution as a result of RHA addition [31]. RHA-I adsorbs generally more Calcium ions from the lime solution due to its higher S_{BET}, resulting in a higher electrical variation. So, it is as a consequence classified as a highly pozzolanic material. On the other hand, RHA-II is classified as moderately pozzolanic.

Bamboo-Pulp-reinforced cement composites

The composites were obtained by the slurry-dewatering-compaction method simulating, in laboratory scale, the industrial process for fibrecements production [32]. A refined Kraft bamboo pulp with an average fibre length of

Table 1 Chemical composition and physical properties of RHA and OPC

	RHA-I	RHA-II	OPC
SiO_2 (%)	73.6	94.6	17.9
C (LOI) (%)	22.9	1.4	1.6
Al_2O_3 (%)	0.075	0.085	4.85
Fe_2O_3 (%)	0.255	0.145	2.7
MgO (%)	0.27	0.280	2.15
CaO (%)	0.755	0.925	64.45
Na_2O (%)	0.09	0.055	0.3
K_2O (%)	1.165	1.115	–
SO_3 (%)	–	–	2.4
ΔmS/cm	1.4	0.58	–
S_{BET} (m^2/g)	119	15	–
δ (μm)	1.8	4.0	–

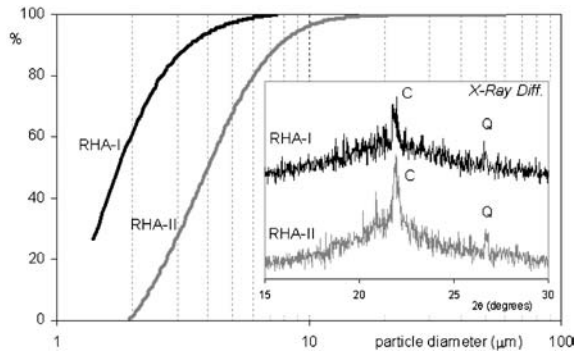

Fig. 1 Particles size distributions and X-Ray diffraction results of RHA-I and II

1.47 mm was employed at a fixed ration of 8% by dry mass of the binder. The OPC employed was an ENCI cement quality 32.5R (similar to an ASTM type I Portland cement), of which the composition is given in Table 1.

Partial cement replacements by RHA amounted 15% and 30%; the different compositions of the specimens and their mix codes being displayed in Table 2. The majority of composites specimens were cured in a sealed plastic bag for 7 days, and then exposed to the open air for the rest of the curing period. This procedure is considered as the standard curing method. For the composites subjected to accelerated autoclave curing (8 h at 175 °C, 1 MPa), an ''A'' is added to the mix code. For comparison, plain cement matrices were similarly produced and, in this case, only RHA-I was employed as a cement replacement material.

Experimental

MIP tests

A Micromeritics PoreSizer 9320 performed the MIP tests six months after the production of the composites and pastes, with pressure varying from 0 MPa to 205 MPa. An equilibrium period of 30 s was included in the procedure at each pressure increment before recording the pressure and intruded Hg volume data. Values of $\gamma = 485$ dyn/cm^2 (0.1 Pa) and, based on commonly used values for contact surface angle between Hg and cement, $\theta = 141°$, were adopted in Eq. (1). For comparative purposes, the intrusion values are expressed in percentage of the bulk volume of the sample.

Permeability of RHA-blended-cement pastes and composites

The permeability of pastes and composites was determined by K–T and C–C methods on the basis of the intrusion curves obtained from MIP tests. Determination of the volume fraction of C–S–H, ϕ_{CSH}, for assessment of K_L in the C–C method, requires estimation of V_{CSH}/V_{CH}. For a range of different cement pastes (*w/c* ratios of 0.3 and 0.4, and hydration periods from 7 to 210 days) reported [26], a fixed V_{CSH}/V_{CH} value of 2.63 was applied. The same value is used in this study for non-blended pastes and composites (M0 and CP0). For the other composites, it is assumed that the added RHA consumes all CH, so $V_{CH} = 0$. The composites were produced by the laboratory-scale Hatschek method, without a fixed *w/c*. However, a random check after the slurry-dewatering-compaction process yielded the *w/c* ratio to be about 0.3, which is the value applied in the calculations for all blended composites.

Table 2 Composition and mix code of the samples

Mix code	Binding (% dry mass)			Pulp (% binding)
	OPC	RHA-I	RHA-II	
M0	100	0	0	0
M15	85	15	0	0
M30	70	30	0	0
CP0	100	0	0	8
CP15-I	85	15	0	8
CP30-I	70	30	0	8
CP15-II	85	0	15	8
CP30-II	70	0	30	8
CP30-IA	70	30	0	8

Experimental evaluation of permeability

The permeability of some of the composites considered in the porosity analysis was determined experimentally applying a diffusion cell originally developed for the study of transport phenomena in sedimentary rocks [33]. Disks with a thickness of 6 mm thick and a diameter of 38.1 mm were cut from the composite plates and placed between two caps that were connected to the pressure pump and the pressure transducers, so that the pressure on both upper and lower surfaces of the sample could be continuously recorded. The set-up of the sample in the diffusion cell is depicted in Fig. 2a. The layers of porous stone between the sample and the caps are for adjustment of the sample thickness in the equipment, while the polyester cloth added between the porous stone layer and cap at the top of the sample compensates for small irregularities in the thickness of the sample. This guarantees a perfect match between the upper cap and the rest of the set-up. Unidirectional water flow through the sample thickness was applied by the pump. This condition was guaranteed by using a thermo-retractable rubber layer around the whole set-up, perfectly adjusted after submitting to heat. A metallic wire tightened the two ends for extra security (Fig. 2b). The diffusion cell was thereupon closed and filled with oil (Fig. 2c). This allowed submitting the set-up to a constant confining pressure of 3.0 MPa during the tests. Permeability can be calculated by Darcy's law after arriving at the laminar flow condition under constant flow rate, Eq. (2). The main inconvenience of this procedure is the long period required to achieve the laminar flow through low permeability materials. A method to determine permeability before the laminar flow condition is established combines experimental results and numerical modelling [33].

The upper surface of the sample is subjected during the test to a constant water pressure, whereby the pressure transducers record the way this pressure is transmitted to the lower surface. In the numerical analysis, the sample is

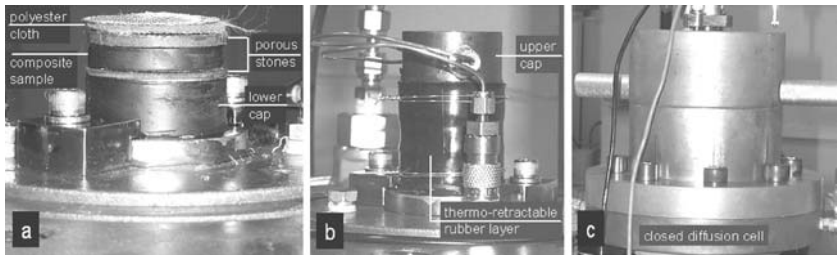

Fig. 2 General set-up of the permeability test: (**a**) the composite sample is placed between porous stones, (**b**) the system is hindered laterally with a thermo-retractable rubber layer, and (**c**) the diffusion cell is closed filled with oil,

approximated by a finite element network, whereupon the numerical calculations are performed using the FPORO program developed by the Petroleum Engineering and Technology Group (GTEP/PUC-Rio) for permeability studies of rocks on the basis of Darcy's law. As input data, the program requires information on the pressure imposed experimentally, as well as on some physical properties of the sample and of the applied fluid, including an initial value for permeability. The output of the numerical calculation is a curve representing the variation of the pressure on the lower surface of the sample due to the imposed pressure on the opposite surface. An iterative procedure is carried out whereby the input value of the permeability is step-wise upgraded until the best correlation between the numerical and experimental curves is achieved [34].

Results

MIP tests

Table 3 presents the physical properties of the composites as derived from the MIP tests. Bulk density is the mass per unit volume of the material with pores. The skeletal density is the mass per unit volume of the pore-free material, *i.e.*, ignoring the pores intruded by mercury. The maximum cumulative intrusion volume is given in relation to sample mass. The total porosity is the ratio of maximum intrusion volume and bulk volume of the sample. Relying on the reproducibility of the method [19, 20], only one sample was tested per composition. Exceptions are plain paste M15-I and composite CP15-II, of which two samples were analyzed. Table 3 confirms these repeated tests to have yielded close values for the properties calculated from these tests. Also, the intrusion curves of these samples were almost identical, supporting the reliability of the single-sample set up.

Figure 3 presents the incremental and cumulative intrusion curves of the plain cement matrix M0 and plain composite CP0. The intrusion curves of M0 follow the general trend indicated in the literature for cement pastes, with no significant intrusion being detected for pores larger than about 0.2 μm and with an intrusion peak occurring at this very level. This intrusion peak indicates the presence of an inter-connected pore network and allows defining a characteristic pore size, the threshold, or critical, pore diameter [14, 16, 17]. The threshold pore diameter is regarded as an intrinsic characteristic of cement pastes, being independent of the water/cement ratio [35]. Pores in the 0.05 μm to 0.15 μm range contribute by about 60% to porosity of M0. A prominent peak at 0.12 μm implies 11% of all pores in the sample to have a similar size. The pores smaller than 0.05 μm account for about 21% of total porosity.

The intrusion curves of CP0 reveal (Fig. 3) pores larger than 0.15 μm responsible for the difference between the pore structures of paste and composite. While in the paste these pores contribute to about 8.5% of the total porosity, in the composites they do so for almost 50%. The four peaks occurring at pore diameters of 0.2, 0.25, 0.3 and 0.4 μm compose a pattern reproduced in all composites tested in this study. Since pores smaller than 0.15 μm are related to the matrix structure, and the main changes due to RHA addition are observed in the range of pores smaller than 0.4 μm, these peaks are probably coming from pores in the interfacial transition zone, reflecting a gradual pore refinement from the region closer to the fibres to the pore network of the bulk matrix.

The intrusion curves in Fig. 4 show the effects of the addition of 30% RHA-I on the pore structure of the composites. It can be observed that the blended-cement com-

Table 3 Physical properties resulted from MIP tests

Sample composition	Bulk density (kg/m^3)	Skeletal density (kg/m^3)	Max. Cum. Int. Vol. (m^3/kg) ($\times 10^{-3}$)	Porosity (%)
M0	1972.1	2297.4	0.072	14.2
M15-I (a)	1778.1	2148.7	0.097	17.2
M15-I (b)	1779.9	2135.2	0.094	16.6
M15-I (mean)	1779.0	2142.0	0.095	16.9
M30-I	1628.3	1951.5	0.102	16.6
CP0	1613.1	2146.3	0.154	24.8
CP15-I	1505.0	2013.5	0.168	25.3
CP30-I	1361.5	1829.6	0.188	25.6
CP15-II (a)	1504.6	1968.0	0.157	23.5
CP15-II (b)	1479.7	1930.4	0.159	23.3
CP15-II (mean)	1492.2	1949.2	0.157	23.4
CP30-II	1503.2	1912.2	0.142	21.4
CP30-IA	1376.0	1834.7	0.182	25.0

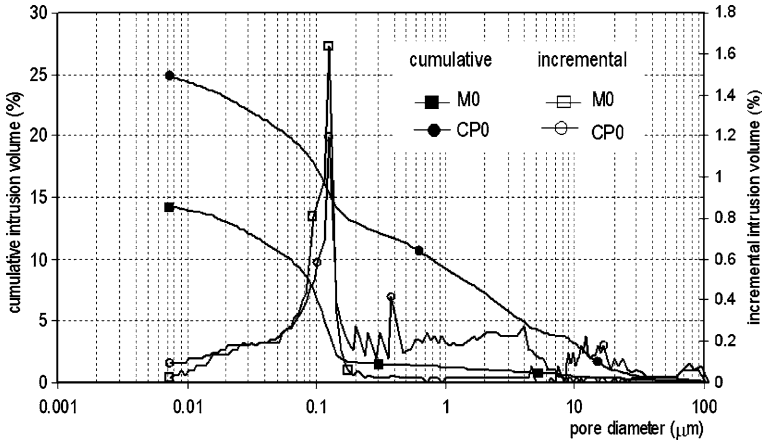

Fig. 3 Comparative intrusion curves of matrix (M0) and composite (CP0)

posites have relatively high volume of pores larger than 0.15 μm, distributed in a similar pattern as that observed in the plain composite. The main effects of RHA-I can be observed on pores smaller than 0.15 μm, which are characteristic of the matrix. The blended-cement composites show lower volume of pores with diameter between 0.05 and 0.15 μm. The reduced porosity of the matrix is probably an effect of the pozzolanic reaction, with its products blocking the pore network. Additionally, the intrusion curves from samples of composites with 15% and 30% RHA presented similar features; therefore, only the intrusion curves from composites with 30% RHA are shown.

In relation to CP0, the addition of RHA-II decreases both density and porosity of the composites (Table 3). It is revealed in Fig. 5 that 30% RHA-II decreases the porosity related to the localized peaks (interface) and, mainly, that related to the matrix. Instead of the intrusion peak that characterizes the threshold diameter of the matrix in the plain-cement composite, the blended-cement composites present intrusion levels remarkably lower. Again, once the RHA particles are larger than the pores in the refined range (0.08–0.3 μm) this refinement may be the effect of porosity blocking by the products of the pozzolanic reaction, which seems to be enhanced by the decreased carbon content in RHA-II.

Although the small changes in density and porosity values in Table 3 suggest little influence of the curing process on the pore characteristics of the composites, the intrusion curves in Fig. 6 show the opposite. The effects of autoclave curing on pore characteristics of composites with RHA-I are similar to those resulting from addition of RHA-II in composites under standard curing, as presented in Fig. 5. A refinement of porosity in the interfacial region, and a strong modification in the size distribution of the pores of the matrix are observed in Fig. 6. Pore sizes around the threshold level are responsible for only a modest intrusion volume, but there is an increase in the intrusion rates at finer pore levels, showing the refinement of the matrix due to the autoclave process.

Calculated permeability of cement pastes and composites

A large discrepancy between the results obtained from the C–C and K–T models, can be seen in Table 4. Comparing the obtained results in Fig. 7, with those from the available

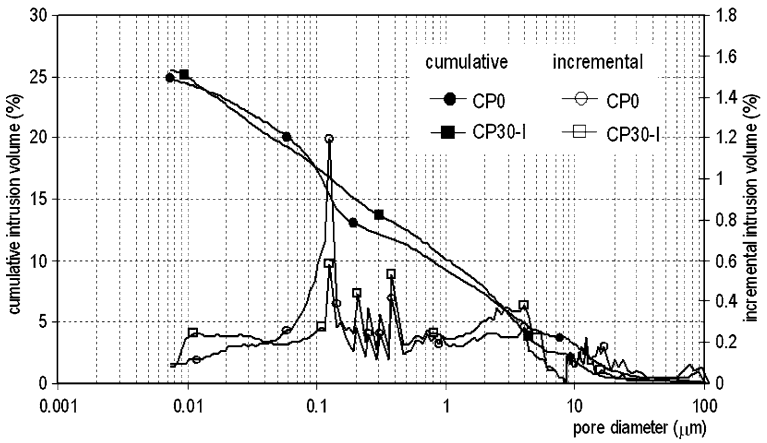

Fig. 4 Effects of RHA-I incorporation on the pores distribution of composites

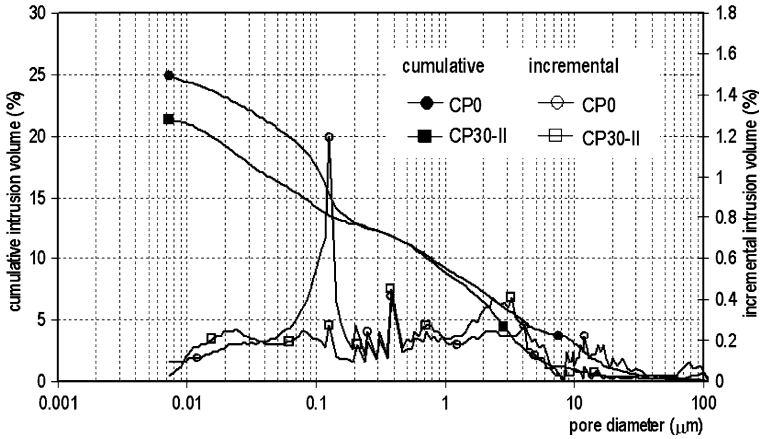

Fig. 5 Effects of RHA-II incorporation on the pores distribution of composites

published data, indicates that the C–C model represents the matrix' permeability more realistically. The K–T model results in permeability, about 10^{-19} m^2, that is, about 10 times higher than data reported for pastes with w/c of 0.25 and 0.36 and hydrated for 182 days, 0.4×10^{-20} m^2 and 10^{-20} m^2, respectively [21]. The latter value is in the same order of magnitude as the permeability data for 28-days-old cement pastes with *w/c* of 0.47 [25]. However, after 210 days, cement pastes with *w/c* of 0.3 and 0.4 presented permeabilities of 2.8×10^{-23} and 1.3×10^{-22} m^2, respectively [26]. Furthermore, it should be noted that total porosities of the cement pastes reported are lower than the critical value of 18%, defined by Garboczi and Bentz [28] as the value below which connectivity of the pores decreases sharply. Based on the presented data it can be assumed that the C–C model better represents the permeability of the cement pastes. It could be concluded that the addition of RHA-I does not modify significantly the permeability of the cement pastes, in the order of 10^{-22} m^2.

For the studied cement pastes, the threshold diameter, d_c, is easily identified, as far as almost no significant intrusion is observed in pores larger than d_c. The intrusion curves of the bamboo-pulp-reinforced composites are more complex, reflecting features characterizing the matrix, the interface and the reinforcement. The complexity of the pore structure makes it difficult to define a single parameter that would represent realistically the whole pore network. As a first approximation, the threshold diameter of the composite can be assumed similar as that of the matrix (about 0.1 μm), whereas the additional porosity resulting from the incorporation of the reinforcement will consist of larger pores in the same network. This rendered possible calculating by K–T and C–C models the permeability data listed in Table 4 and plotted in Fig. 7.

Data regarding a commercial cellulose–cement composite reported in the literature [7] refers to permeability to Nitrogen at the level of 10^{-18} m^2. The K–T model results values of the same order of magnitude. However, the results are almost the same for all composites considered, showing that the refinements in the pore structure observed in some composites do not influence permeability. The C–C model is more sensible to variations in pore structure of the composites. However, the measured permeability of the composites can be considered too low when compared to permeability for cement pastes reported in the literature [21, 25, 26] and to the aforementioned information presented for cellulose–cement composites [7].

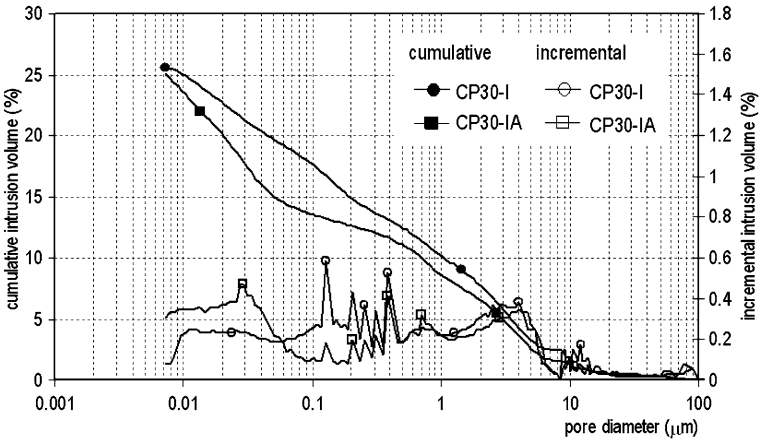

Fig. 6 Effects of accelerated autoclave curing on the pores distribution of composites with RHA-I

Table 4 Calculated permeability of pastes and composites through analytical models

	d_c (μm)	ϕ	K–T model				C–C model							
			d^e_{max} (μm)	$S(d^e_{max})$	(σ/σ_0)	K (m^2) $\times 10^{-20}$	ϕ_c	α	V_{CSH}	V_{nH}	ϕ_{CSH}	K_H (m^2) $\times 10^{-16}$	K_L (m^2) $\times 10^{-23}$	K (m^2) $\times 10^{-20}$
M0	0.11	0.14	0.04	0.11	0.0055	29.225	0.06	0.73	0.84	0.12	0.87	0.79	4.14	0.009
M15-I	0.10	0.17	0.04	0.12	0.0069	32.126	0.04	0.76	0.84	0.12	0.87	0.67	5.00	0.009
M30-I	0.08	0.17	0.03	0.12	0.0065	19.832	0.06	0.74	0.81	0.14	0.86	0.45	4.79	0.009
CP0	0.13	0.25	0.043	0.21	0.0177	125.263	0.15	0.57	0.45	0.22	0.67	1.04	2.54	0.081
CP15-I	0.13	0.25	0.043	0.21	0.0182	128.297	0.17	0.54	0.60	0.23	0.72	1.04	3.05	0.446
CP30-I	0.13	0.26	0.043	0.20	0.0174	122.436	0.17	0.54	0.60	0.23	0.72	1.04	3.05	0.446
CP15-II	0.13	0.23	0.043	0.19	0.0155	109.002	0.16	0.56	0.61	0.23	0.73	1.04	3.15	0.192
CP30-II	0.13	0.21	0.043	0.17	0.0120	84.871	0.14	0.60	0.65	0.21	0.76	1.04	3.51	0.066
CP30-IA	0.13	0.25	0.043	0.16	0.0134	94.253	0.13	0.61	0.66	0.20	0.77	1.04	3.60	0.045

Analysing the intrusion curves of the composites, Figs. 3–6, and the models for permeabilty, it can be observed that when larger pores are regarded as d_c, the discrepancies between the results of the two analytical models increase. The scale of the threshold diameter in Eq. (3) defines the magnitude of the results of the K–T model. As a consequence, larger threshold diameters will result in higher permeability. On the other hand, the magnitude of the permeability in the C–C model depends mainly on the porosity adopted in the effective media equation. In Eq. (5) the porosity is a weight function reflecting the relative importance of the low and high permeability phases. In the cumulative intrusion curves, larger threshold diameters correspond to lower porosity, which in turn enhances the contribution of the low permeability phase in Eq. (5), resulting in the lower values of permeability. The analytical models therefore fail to predict the permeability of the composites, in the cases studied.

Modified model for permeability of composites

To obtain more realistic results for the permeability of the composites, a modified analytical model is proposed. It is also based on the effective media theory, considering the properties of the intrusion curves of the composites. It considers porosity due to pores larger than 0.2 μm as related to the interface zones and to the reinforcement, being the high permeability phase, K^*_H, and the porosity corresponding to the matrix being the low permeability phase, K^*_L, as shown in Fig. 8. This modification of the Cui-Cahyadi [26] model is referred to in this study as the C–C* model.

The permeability K^*_H is calculated by means of the K–T model, Eq. (3), with pores of about 5 μm being regarded as d_c, whereby this pore size represents the first deflection of the cumulative intrusion curves of all composites, *i.e.* interconnected larger pores. For the determination of K^*_L, the C–C model is applied, Eqs. (4) to (6), in which the pore structure is considered consisting of pores smaller than 0.2 μm, and with a threshold diameter equal to that of the matrix. Once K^*_H and K^*_L are established, the permeability of the composite is calculated by Eq. (4). By definition, the porosity, ϕ, in Eq. (4) is that of the high permeability phase. This sub-division in the pore structure in the C–C* model indicates that ϕ should be composed of pores larger than 0.2 μm. However, it is stated that changes in the permeability of cement pastes due to blending occur as a result of the refinement of their pore structure, *i.e.*, by

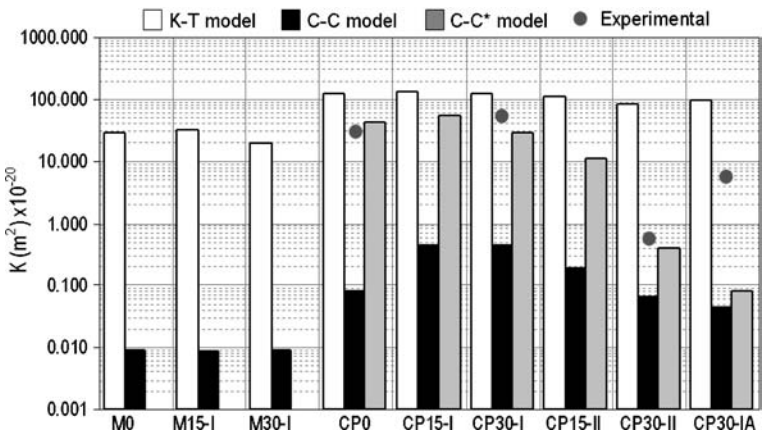

Fig. 7 Comparative values for the permeabilities of matrix and composites

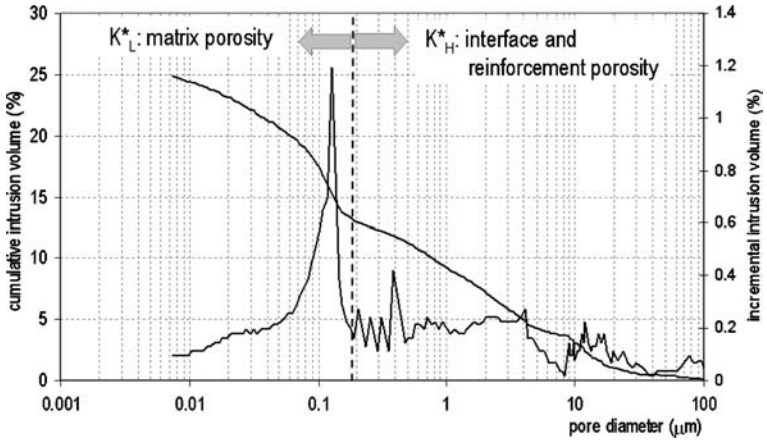

Fig. 8 Low and high permeability phases of cement composites considered in the modified analytical model

decreasing the volume of the macro pores and by increasing the volume of meso pores [14]. When this is taken into account, the border between macro and meso pores can be considered the minimum pore diameter of capillary porosity, whereby ϕ is associated with pores larger than 0.05 μm.

The results from the C–C* model are shown in Table 5 and in Fig. 7. It can be observed that differences with the data reported in the literature [7] are reduced. The model is also sensitive to the refinement of the pore structure resulting from the addition of RHA-II, and to the autoclave curing. These modifications lead to 1000 times lower permeability data of the order of about 10^{-21} m^2.

Experimental determination of permeability

By applying a constant pressure on the upper surface of the sample (P. Top), and observing the different rates at which this pressure is transmitted to the lower surface (P. Bottom), it is possible to evaluate qualitatively how the different pore structures influence the transport properties of the composites. Fig. 9a–d presents information on pressure variations with time on both upper and lower surfaces of the composites for three different consecutive pressure levels. It can be seen that the pressure transmission from the upper surface to the opposite one occurred in a similar manner in normal-cured composites with and without RHA-I, CP0 and CP30-I, respectively, Fig. 9a, b. A lower transmission rate is observed in the autoclaved composite, CP30-IA, Fig. 9c, showing that this composite presents a significantly lower permeability. For the blended composites containing 30% low-carbon-content RHA, CP30-II, Fig. 9d, it was observed that the pressure is transmitted through the sample at a much lower rate than in the other composites, demonstrating the transport properties of the composite to be strongly influenced by the addition of this type of RHA.

Permeability of the composites was assessed by means of the FPORO program, based on the experimental curves obtained in the diffusion cell. In Fig. 9a–d it can be seen that the curves resulting from the numerical calculations are well correlated to those obtained experimentally. The permeability values that generate these numerical curves are presented in Table 6 and Fig. 7, demonstrating the addition of 30% RHA-I slightly to increase permeability of the composites.

MIP tests revealed that autoclaved composites with high-carbon-content RHA and composites with low-carbon-content RHA submitted to standard curing have pore structures with similar characteristics, with a refined porosity in the phases related to the interface zones and to the matrix, Figs. 5 and 6. Based on such pore characteristics,

Table 5 Permeabilities calculated by the modified analytical model

	K^*_H: K–T model						K^*_L: C–C model									C–C* model	
	d_c (μm)	ϕ	d^e_{max} (μm)	$S(d^e_{max})$	(σ/σ_0)	K^*_H (m^2) × 10^{-16}	d_c (μm)	ϕ_c	α	V_{CSH}	V_{nH}	ϕ_{CSH}	K_H (m^2) × 10^{-16}	K_L (m^2) × 10^{-23}	K^*_L (m^2) × 10^{-23}	ϕ*	K* (m^2) × $10^{-2°}$
CP0	4.00	0.13	1.36	0.08	0.004	2.66	0.13	0.04	0.76	0.84	0.12	0.87	1.04	5.03	8.30	0.21	43.000
CP15-I	4.00	0.15	1.36	0.09	0.005	3.39	0.13	0.04	0.77	0.84	0.12	0.88	1.04	5.06	8.30	0.21	53.800
CP30-I	4.00	0.15	1.36	0.09	0.005	3.40	0.13	0.04	0.76	0.84	0.12	0.87	1.04	5.01	8.30	0.20	28.000
CP15-II	3.50	0.16	1.19	0.11	0.006	3.29	0.13	0.02	0.80	0.88	0.10	0.90	1.04	5.36	6.80	0.19	10.900
CP30-II	3.00	0.13	1.02	0.09	0.004	1.55	0.13	0.02	0.79	0.87	0.11	0.89	1.04	5.26	6.70	0.16	0.390
CP30-IA	4.00	0.13	1.36	0.08	0.003	2.38	0.13	0.02	0.80	0.88	0.10	0.89	1.04	5.33	6.70	0.15	0.083

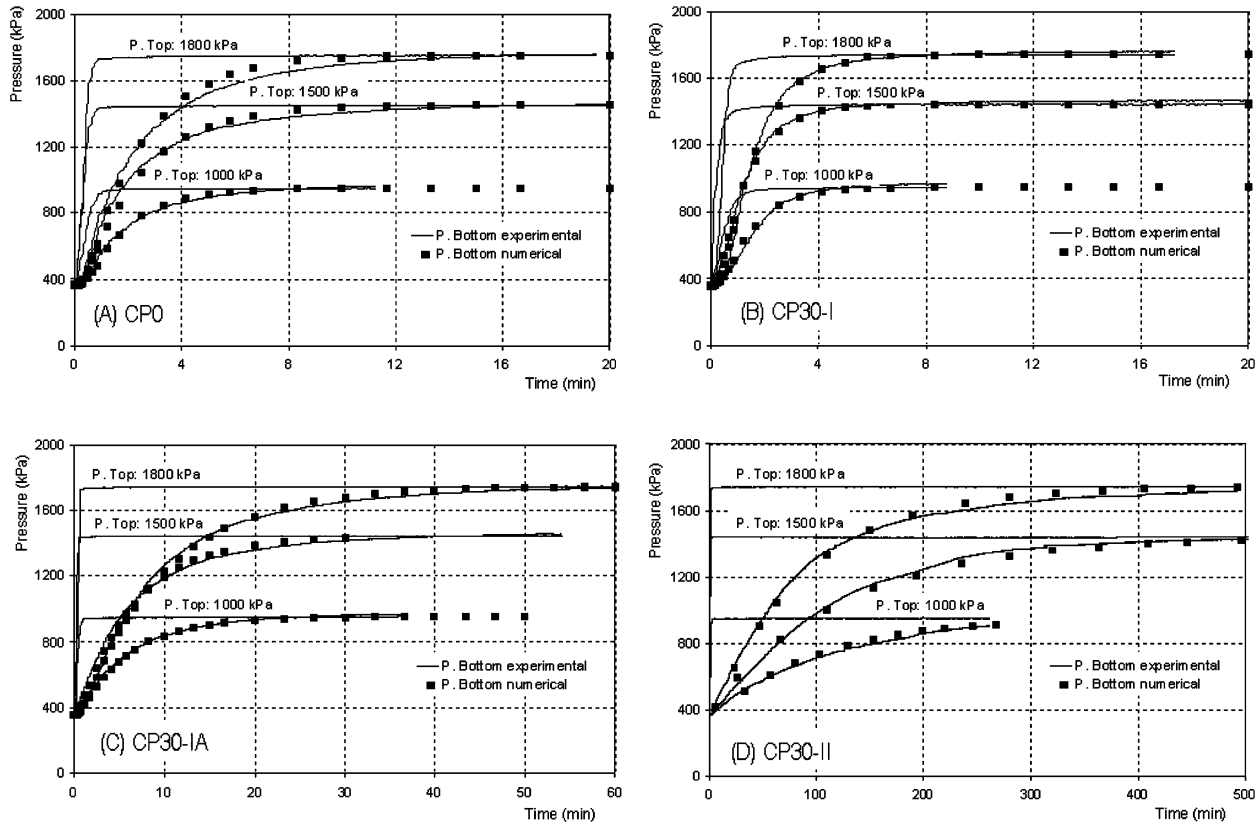

Fig. 9 Pressure transmission curves resulted from the permeability tests

it could be expected that composites CP30-IA and CP30-II would yield according to the modified analytical model close values for permeability, *i.e.*, lower than that of the other samples. However, it is observed that permeability of composite CP30-II is much lower than that of the autoclaved composite CP30-IA. This obvious mismatch could be due to the roughness of the pore surfaces resulting from different curing conditions. Moreover, porosity measurements were performed under quasi-static conditions, while permeability tests were conducted in a situation of dynamic water flow. As a result, crystallization of hydration products at autoclave curing may lead to smoother pores surfaces (lower tortuosity), offering a lower resistance to water movement during the permeability tests. On the other hand, the normal cured CP30-II may feature more irregularly shaped pores surfaces (higher tortuosity), reflected by reduced permeability.

Concluding remarks

This comparative study offers supporting evidence for using MIP, in spite of all limitations, as a valuable tool in assessing modifying effects of mineral admixtures and curing conditions on pore characteristics of cement composites. The main conclusions as to these effects are the following:

- The different replacement rates of OPC by RHA applied (15% and 30% RHA) exert little influence on the pore structure of the composites as reflected by comparable intrusion curves.
- Density is reduced and porosity increased when high-carbon-content RHA (RHA-I) is incorporated in the composites. Total porosity increases probably as a consequence of high porosity in the surface layer of the ash particles. Cement composites blended with this ash yield higher volume of pores exceeding 0.15 μm and lower volume of pores at the threshold diameter of the matrix, demonstrating the modest refinement in the pore structure of the matrix.
- Addition of low-carbon RHA (RHA-II) strongly modifies the pore size distribution in the interface zones and in the matrix, leading to an overall refinement. The decreased porosity probably results from the enhanced chemical interaction between the low-carbon-content RHA and the cement in the matrix.
- Results of the different RHA on the pore structure of cellulose–cement composites seem related to their different pozzolanic activities, since the more significant differences are observed in the pore range smaller than

Table 6 Permeabilities established through the coupled experimental-numerical solution

Sample	P Top (kPa)	K (m^2) $\times 10^{-2}$	K_{mean} (m^2) $\times 10^{-2}$
CP0	1800	18.50	21.0
	1500	18.50	
	1000	26.0	
CP30-I	1800	35.0	38.0
	1500	40.0	
	1000	4.00	
CP30-IA	1800	4.50	6.17
	1500	6.50	
	1000	7.50	
CP30-II	1800	0.45	0.38
	1500	0.30	
	1000	0.40	

the RHA particles. As a consequence, the higher pozzolanic activity (of RHA-II) results in a higher amount of reaction products that decreases the porosity by deposition. This opposes to the results in Table 1, which presents RHA-I as more reactive. Due to its higher S_{BET} value, and the consequent adsorption of more Calcium ions, RHA-I results in more variation in the electrical conductivity of the saturated lime solution than RHA-II. However, it does not mean that all the adsorbed Calcium reacts with the silica in the ash. The more pronounced effects of RHA-II on the pore network and permeability of the composites, despite its larger particles, lower S_{BET} and higher crystalline silica content, shows that higher carbon content may prevent a proper pozzolanic reaction between the mineral admixture and cement reaction products.

- Blending with high-carbon-content RHA can yield similar effects as observed with RHA-II-blended composites provided they are subjected to accelerated autoclave curing.
- Based on general features of the intrusion curves observed for all composites, it is proposed to sub-divide pore structure in three phases: pores with diameters larger than 0.5 μm, introduced by the reinforcement; pores in the 0.2 and 0.5 μm diameter range, which would represent the interfacial zones, and pores smaller than 0.2 μm, characterizing the porosity of the matrix.

Regarding the relation between the pore network and the permeability of the cement composites, the analytical approaches presented in the literature, originally developed for permeability prediction of rocks and cement pastes, were not properly correlated to the features reflected by the intrusion curves of the composites. A modification on these models resulted in more realistic estimates for the permeability, agreeing with the experimental results of normal-cured composites. However, for autoclaved composites, the experimental permeability does not correspond to the value obtained from the analytical model. This is probably due to different pore surface characteristics resulted from the autoclaved curing, with the composites showing a similar pores distribution to that of some normal cured composites (during the quasi-static MIP test) and quite different permeability behaviour (during the dynamic diffusion test).

Finally, the porosity and permeability results allow a better insight into mechanisms to improve by RHA incorporation the durability of composites. The porosity of matrix and interface is decreased, reducing water permeability, probably preventing or minimizing the effects of the main transport-related deterioration mechanisms affecting these composites under normal service life conditions. In this sense, best performance is expected from normal cured composites blended with low-carbon RHA.

Acknowledgements This study was financially supported by CNPq–National Council for Scientific and Technology Development, Brazilian Ministry of Science and Technology, and was developed at Delft University of Technology as a cooperation project supported by CICAT–Management Centre for International Cooperation. The authors are grateful to Doctor Eudes Siqueira Muniz, from the Petroleum Engineering and Technology Group-GTEP/PUC-Rio, for making possible the experimental study on permeability with the diffusion cell.

References

1. Studinka JB (1989) Int J Cem Lightweight Concr 11:73
2. Coutts RSP (1988) In: Swamy RN (ed) Natural fibre reinforced cement and concrete. Blackie and Son Ltd, Glasgow, 1pp
3. Sharman WR, Vautier BP (1986) Dur Build Mat 3:255
4. Gram HS, Persson H, Skarendhal A (1984) In: Natural Fibre Concrete (SAREC, Stockholm) 5pp
5. Soroushian P, Marikunte S (1984) In: Daniel JI, Shah SP (eds) Fiber reinforced concrete: developments and innovations. American Concrete Institute, 73pp
6. Canovas ME, Selva NH, Kawiche GM (1992) Mat Struct 25:417
7. Macvicar R, Matuana LM, Balatinecz JJ (1999) Cem Concr Comp 21:189
8. Toledo Filho RD, Ghavami K, England GL, Scrivener K (2003) Cem Concr Comp 25:185
9. Yu Q, Sawayama K, Sugita S, Shoya M, Isojima Y (1999) Cem Concr Res 29:37
10. FAO (2004) In: Rice market monitor, vol VII, issue 4, (Food and Agriculture Organization for the UN, http://www.fao.org/es/ESC/en/20953/21026/highlight_23001en_p.html, 9th Sept)
11. Cook DJ (1986) In: Swamy RN (ed) Cement replacement materials. Blackie & Son Ltd, London, 171pp
12. Stroeven P, Bui DD, Sabuni E (1999) Fuel 78:153
13. Bui DD (2001) In: Rice husk ash as a mineral admixture for high performance concrete, Delft University Press, Delft, 13pp
14. Brown PH, Shy D, Skalny J (1991) In: Skalny J, Mindess S (eds) Materials science of concrete II. The American Ceramic Soc. Inc, 83pp
15. Aldea CM, Young F, Wang K, Shah SP (2000) Cem Concr Res 30:465
16. Metha PK, Monteiro JP (1993) In: Concrete: structure, properties and methods. Prentice Hall, New Jersey, 26pp
17. Winslow DN, Lovell CW (1981) Powder Tech 29:151

18. Diamond S (2000) Cem Concr Res 30:1517
19. Ye G (2003) In: Experimental study & numerical simulation of the development of the microstructure and permeability of cementitious materials. Delft University Press, Delft, 43pp
20. Hedenblad G (1997) Adv Cem Based Mat 6:123
21. El-Dieb AS, Hooton RD (1994) Cem Concr Res 24:443
22. Banthia N, Mindess S (1989) Cem Concr Res 19:727
23. Katz AJ, Thompson AH (1986) Phys Rev B 34:8179
24. Tumidajski PJ, Lin B (1998) Cem Concr Res 28:643
25. Christensen BJ, Mason TO, Jennings HM (1996) Cem Concr Res 26:1325
26. Cui L, Cahyadi JH (2001) Cem Concr Res 31:277
27. Garboczi EJ (1990) Cem Concr Res 20:591
28. Garboczi EJ, Bentz DP (1996) Constr Build Mat 10:293
29. Bentz DP, Garboczi EJ (1991) Cem Concr Res 21:325
30. Allen T, Marshall K (1972) In: The electrical sensing zone method of particle size measurement: the Coulter principle. University of Bradford, England, 105pp
31. Luxán MP, Madruga F, Saavedra J (1989) Cem Concr Res 19:63
32. Campbell MD, Coutts RSP (1980) J Mat Sci 15:1962
33. Muniz ES (2003) In: Desenvolvimento de Equipamento e Metodologia de Testes para Avaliação da Interação Folhelho-Fluido de Perfuração. Doctorate thesis, Pontifícia Universidade Católica do Rio de Janeiro, Rio de Janeiro, in Portuguese, 41pp
34. Frydman M, Fontoura SAB (2001) In: Proceedings of the Latin American and Caribbean Petroleum Engineering Conference. Buenos Ayres, 8pp
35. Matte V, Moranville M (1999) Cem Concr Comp 21:1